Manufacturing thin ionic polymer metal composite for sensing at the microscale

Motreuil Ragot, Paul; Hunt, Andres; Sacco, Leandro Nicolas; Sarro, Pasqualina Maria; Mastrangeli, Massimo

DOI
10.1088/1361-665X/acb305

Publication date
2023

Document Version
Final published version

Published in
Smart Materials and Structures

Manufacturing thin ionic polymer metal composite for sensing at the microscale

OPEN ACCESS
IOP Publishing
Smart Materials and Structures
Smart Mater. Struct. **32** (2023) 035006 (11pp)
https://doi.org/10.1088/1361-665X/acb305

Manufacturing thin ionic polymer metal composite for sensing at the microscale

Paul Motreuil Ragot*, Andres Hunt, Leandro Nicolas Sacco, Pasqualina Maria Sarro and Massimo Mastrangeli

Microelectronics, Delft University of Technology Faculty of Electrical Engineering Mathematics and Computer Science, Mekelweg 4, Delft, Zuid-Holland, 2628 CD, The Netherlands

E-mail: P.A.Motreuil-Ragot@tudelft.nl

Received 10 June 2022, revised 12 December 2022
Accepted for publication 13 January 2023
Published 30 January 2023

Abstract

Ionic polymer metal composites (IPMCs) are a class of materials with a rising appeal in biological micro-electromechanical systems (bio-MEMS) due to their unique properties (low voltage output, bio-compatibility, affinity with ionic medium). While tailoring and improving actuation capabilities of IPMCs is a key motivator in almost all IPMC manufacturing reports, very little efforts have been dedicated to sensing using IPMC thinner than 100 μm. Most reports on IPMC manufacturing and utilization rely on 180 μm-thick Nafion with platinum electrodes, too stiff for bio-MEMS applications. The same fabrication process on thinner membranes does yield in very poor electrodes and performance, and needs to be studied to increase flexibility and sensitivity in the microscale range. This study demonstrates an electroless Pt deposition method for fabricating bio-MEMS-suitable 50 μm-thick IPMC samples. First, we perform a comparative study on the platinum distribution within the Nafion backbone as well as on the surface for the standard electroless deposition recipe for thin (50 μm) and thick (180 μm) Nafion. We report strong differences in platinum distribution for thick and thin IPMC that experienced the same manufacturing process. By varying chemical concentrations from the standard recipe we obtain convenient platinum distribution on thin Nafion, with platinum mainly localized in proximity of surface, as well as electrodes with lower sheet resistance. We could measure the flexural rigidity as 3.43×10^{-8} N·m^2, 46 times lower than standard 180 μm-thick IPMC. The calculated sensitivity is 0.476 ± 0.02 mV mm^{-1} and the limit of detection for our sensor is 500 ± 20 μm. This procedure sets a milestone for manufacturing 50 μm-thick IPMC for transducers and sensors in bio-MEMS applications.

Supplementary material for this article is available online

Keywords: ionic polymer metal composite, electroless deposition, transducers, Nafion

(Some figures may appear in colour only in the online journal)

* Author to whom any correspondence should be addressed.

1. Introduction

Ionic polymer metal composites (IPMCs) are a type of ionic electroactive polymers (iEAPs). IPMCs are composed of a water permeable membrane with electrodes on both sides of the membrane. The membrane is most commonly a perfluorinated sulfonic-acid (PFSA) ion-conductive polymer known under the brand name of Nafion. The transport of ions within the membrane due to applied electric field across the electrodes triggers migration of ions together with water molecules. This redistribution in the porous membrane backbone creates internal stress within the polymer, which results in a deformation (figure 1) [1]. The standard and most widely studied approach to manufacture IPMCs uses commercially available Nafion 117 as a starting material (180 μm thick) and platinum as noble metal to be reduced. The standard process of manufacturing IPMC relies on electroless deposition, which consists of reducing noble metal such as gold (Au), platinum (Pt) or palladium (Pd) on the surface of the polymer in order to create mechanically robust and chemically stable electrodes [2]. To date IPMCs have been extensively studied for their good actuation capabilities, therefore IPMCs have been widely employed in soft robotics with a focus on actuation [3, 4]. IPMCs also work as a sensor as deformation of the material leads to a reorganisation of the ions within the polymer (figure 1) [5]. Migration of charges could be monitored with the electrodes using a dedicated electronic circuit to record either current, voltage or charge imbalance produced by the displacement [6]. IPMC has been proposed for many different sensing applications such as velocity, pressure, humidity sensors [7–9].

Besides for soft robotics, IPMCs represent great candidates for biological micro-electromechanical systems (bio-MEMS). In bio-MEMS there is the need to manipulate and sense changes at the micro-scale, requiring to match dimensions and mechanical flexibility of biological samples, applying force in the micro-Newton range and displacement in the micro-meter range. Hence lab-on-chip and organ-on-chip devices can benefit from the integration of IPMCs because of their actuation and sensing capabilities. Utilisation of a 180 μm-thick IPMC has been studied for actuating and sensing in bio-MEMS transducers applications [10], with a focus on sensing intrinsic tissue contraction [11, 12]. However, these studies could not realize measurement of tissue contractions, indicating that the stiffness of the 180 μm-thick IPMC is too high to allow the cultured tissue to induce a displacement on the ionic electroactive polymer.

Manufacturing IPMC for MEMS has been studied by very few reports this far. Most of the already existing reports focus on 180 μm-thick IPMC, in addition sensing has been poorly studied. Yanamori *et al* studied the fabrication of 180 μm-thick palladium-based IPMC for micro systems, as palladium is reported to have lower stiffness and being cheaper than Au or Pt electrodes [13]. Tsuchitani *et al* and Feng *et al* studied the manufacturing of IPMC by using standard MEMS-specific microfabrication techniques in a cleanroom environment with a focus on implementing the fabrication of IPMC on a Si substrate [14, 15]. They were able to manufacture a micro-IPMC by casting Nafion solution. However, the focus was on the standard 180 μm-thick Nafion for Yanamori *et al*, and standard electroless recipe for Tsuchitani *et al* and Feng *et al* leading to too stiff material to obtain low flexural rigidity for sensing applications. Yang *et al* reviewed recent progress in IPMC manufacturing, however there was no report on thin Nafion for micro-scale applications [16]. Wang *et al* studied the effect of IPMC dimensions on IPMC sensing, indicating that thicker IPMCs exhibit stronger sensing signal [17], unfavourable for bio-MEMS applications due to their high stiffness.

Therefore, the gap towards application of IPMC for bio-MEMS lies in fabricating thin IPMCs with low bending stiffness and sufficient sensing and actuation capabilities. Our work proposes the first comparative study of platinum distribution for thin and thick Nafion and a novel method to manufacture thin IPMC based on a diluted recipe. First, the standard fabrication recipe [2] is applied both on standard Nafion 117 (180 μm thick) as well as Nafion 212 membranes and the resulting electrode morphology is studied during and after fabrication. Strong differences in the platinum distribution are shown and tentative explanations given. A correction to the standard recipe is developed to compensate for the behaviour of the Nafion 212 membrane. About 50 μm-thick IPMC samples were fabricated basing on the proposed recipe, and their electrical properties (surface resistance) were characterized as well as sensing capabilities (responsivity) and material characteristics (Young's modulus, flexural rigidity). The achieved sensing capabilities show that this new manufacturing approach could be efficiently used to further develop sensing applications for bio-MEMS such as strain sensor for muscular thin film [18].

2. State-of-the-art manufacturing of IPMC

Prior reports studied the different parameters that can influence the electroless deposition for IPMC manufacturing, such as dimensions, concentration of reducing agents, number of reducing cycles, time and temperature [19–24]. However, little explanation and no comparative studies have been reported on commercially available Nafion 212, which is 3.6 times thinner than Nafion 117 and has the same equivalent weight (1100 g·mol^{-1}).

2.1. Influence of manufacturing parameters

Yip *et al* used the Taguchi method for design of experiments to look for the best IPMC manufacturing parameters. They outlined that a few parameters have a very strong influence on the electroless deposition recipe, such as reducing time and reducing agent concentration [19]. Sode *et al* reported the crucial importance of hydration level as well as pH to control the depth of Pt deposition in thick Nafion [20].

Nakamura *et al*, Oh *et al*, Khmelnitskiy *et al* and Cilingir *et al* studied the influence of thickness for actuation purposes using hot-pressed resin to manufacture Nafion with different thicknesses ranging from 50 μm to 700 μm [21–24].

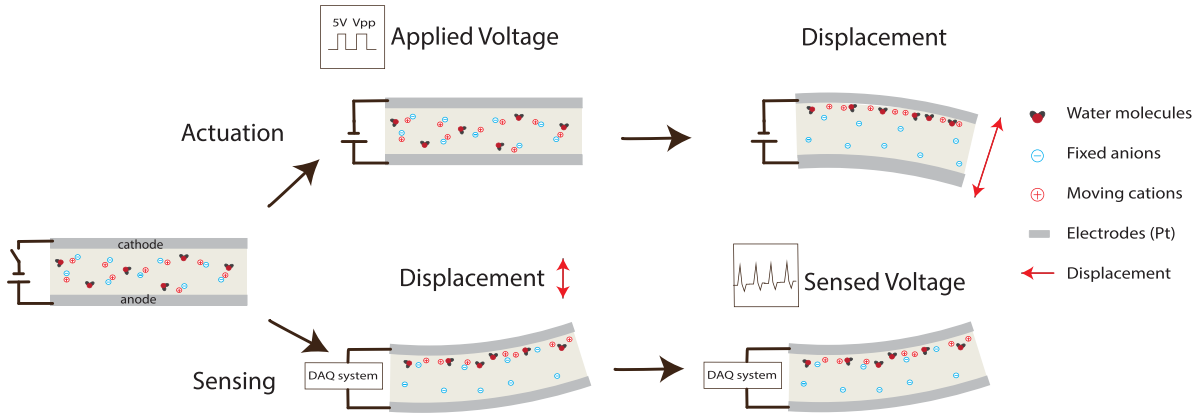

Figure 1. Macroscopic sketch of the cross-section of the IPMC working as actuator and sensor. In the actuation mode (top), the applied voltage will induce a displacement of the polymer. In the sensing mode (bottom), displacement deforms the IPMC substrate, triggering cation migration and causing a charge imbalance, measureable as a voltage difference across the electrodes.

Interestingly Nakamura *et al* and Khmelnitskiy *et al* also showed the influence of cycle and phases repetitions [21, 23]. However Oh *et al* used multi-wall carbon nanotube electrodes, which are not as mechanically robust as the platinum-based electrodes fabricated with the electroless deposition technique, as evidenced by delimination issues [22]. While Cilingir *et al* reported the manufacturing of IPMC using 50 μm-thick Nafion [24] and the standard electroless recipe, leading to 10 μm-thick platinum electrodes, too thick and stiff for bio-MEMS sensing applications.

2.2. Thin Nafion behaviour

IPMC fabrication based on thin Nafion has not been studied in depth, however, insights into the behaviour of Nafion 212 shown in literature attest that thin Nafion behaves differently than thick one. Thin Nafion has been reported to exhibit higher water uptake versus swelling ratio, as well as higher ionic conductivity [20, 25, 26]. Ingle *et al* studied the Pt particles distribution within Nafion 212 for fuel cell membrane manufacturing and with different chemicals than the ones standardly used for IPMC manufacturing [27]. Pak *et al* reported the manufacturing of thin IPMC (Nafion 212) for micropump application, they were the first to introduce the idea to lower the concentration of reducing agent (2/5 of the original reducing agent concentration) [28]. Fuel cell researchers also studied the impact of Pt deposition on very thin perfluorinated membranes, thus Kumar *et al* studied the impact of hydration level on Nafion membranes thinner than 50 μm for fuel cells [29]. While Hawut *et al* and Hosseinabadi *et al* studied the influence of electroless deposition parameters for fuel cell applications [30, 31]. Literature points to dilution as a way to improve platinum electroless deposition on Nafion, however this has not been well described so far for thin IPMC manufacturing.

3. Materials and methods

3.1. Manufacturing of IPMC : standard and modified recipe

Both IPMC substrates, Nafion NRE-212 membrane (thickness 50 μm, Alfa Aesar), here called thin Nafion, as well as the Nafion 117 membrane (thickness 180 μm, Alfa Aesar), here called thick Nafion, were manufactured by electroless deposition of platinum, following the standard recipe described in [2]. The two Nafion membranes have the same equivalent weight (1100 g·mol^{-1}). All chemicals have been purchased from Sigma Aldrich and used as received.

Manufacturing of the IPMCs consists of two phases. The first phase is meant to deposit platinum within the Nafion boundary layer and involves the immersion of Nafion within the platinum organo-metallic solution followed by the reduction of platinum using sodium borohydrade (NaBH4). The reduction is repeated 8 times at temperatures increasing from 40 °C to 60 °C. These immersion-reduction steps are repeated three times and constitute the initial composition process.

- Initial composition process
  - Incorporate the tetra-amine platinum chloride Pt(NH3)4HCl into the Nafion membrane by immersion.
  - Reduce the platinum in the membrane using NaBH4 solution (5%) including Polyvinyl-pyrrolidone PVP10 (0.001 M) for miscibility.

Afterwards a final plating step is conducted, called surface electrode growth process. It consists in reducing platinum in the vicinity of the surface, next to the previously grown Pt sites using hydrazine monohydrate (N2H2) and hydroxylamine hydrochloride (HONH2 · HCl). Thus the resistivity of the surface electrodes reduces, giving a final working IPMC.

- Surface electrodes process
  - Prepare a 240 ml aqueous solution containing 120 mg of Pt with 5 ml of 5% ammonium hydroxide.
  - Reduce the platinum on the surface of the Nafion using 5% aqueous solution of hydroxylamine hydrochloride (6 ml) and a 20% solution of hydrazine monohydrate (3 ml).

As already mentioned, Pak *et al* used 2/5 dilution ratio to increase the performance of the IPMC [28]. Therefore, for the altered recipe the immersion bath was left unchanged, while the NaBH4 mass as well as the PVP10 mass were decreased

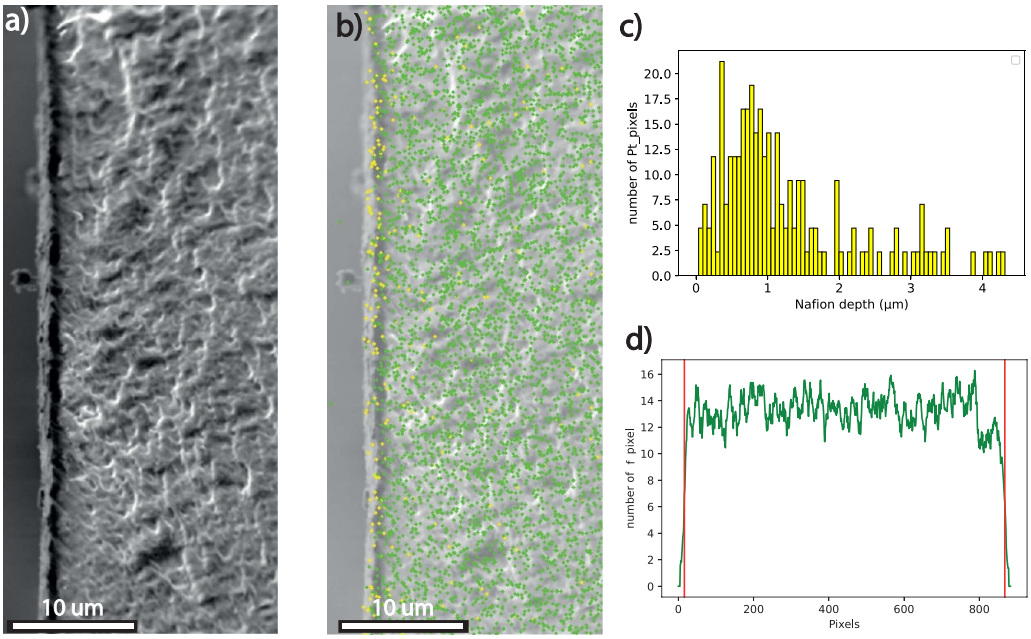

Figure 2. (a) SEM picture of the IPMC cross section (b) SEM picture overlapped with EDS detection map of platinum and fluorine after one reduction step. Green: fluorine, yellow: platinum. (c) Platinum distribution below the surface of Nafion after one reduction step. (d) Fluorine distribution for the entire thickness of the IPMC.

by 60% in the reduction bath using the same amount of water as previously used for the standard recipe (i.e. dilution factor of 0.4). The mass of the reactants used in the final plating of the diluted recipe (hydroxylamine hydrochloride, hydrazine monohydrate and PVP10) was also decreased by the same amount. IPMC cantilever has been cut with laser (Optec) with the following dimensions: L = 18 mm, B = 6 mm. Afterwards the IPMC has been cleaned in an HCl (0.1 M) bath and ions exchanged in phosphate buffered saline solution (PBS), a sodium-based medium commonly used to wash cells and biological samples.

3.2. Analysis of pt distribution in Nafion

Platinum distribution inside Nafion was investigated by using energy-dispersive x-ray spectroscopy (EDS) and image processing. To obtain a clean IPMC cross-section, the IPMC has been immersed in liquid nitrogen and cleaved. Pictures of the cross-section have been taken using scanning electron microscopy (SEM) (Jeol JSM-6010LA) (figures S9 and S10). A region of interest has been extracted in order to select the dedicated area with the electrodes (figure 2(a)). EDS has been used to localize the Pt particles and the Nafion in the cross-section (figure 2(b)). Position of the Pt particles has been extracted using Python 3.6 and Open Computer Vision library (OpenCV) (figure 2(c)). EDS fluorine detection has been used to obtain a precise pixel-to-μm ratio as the thickness of Nafion is known (180 μm or 50 μm) (figure 2(d)). Platinum distribution has been normalized using the amount of fluorine detected in the cross-section for every sample, as fluorine concentration is assumed equal for every sample given the same starting material. The distribution is not meant to be absolute but relative in order to perform comparison from one picture to another.

The detection might be hampered by the shape and focus of the electron beam used for the SEM as well as by the backscattered emission. However from one picture to another we noticed little differences. We assume that the depth of beam penetration might help to compensate for potential non-straight cut of cross-section. Spatial resolution (Zm) of EDS has been estimated using Castaing formula $\mathrm{Zm} = 0.033(E_0^{1.7} - E_C^{1.7})\frac{A}{\rho Z}$, A, being the atomic mass of the element, ρ the density and Z the atomic number. Standard value of Nafion density $\rho = 1.59\,\mathrm{kg\,m^{-3}}$ was used. The minimum emission voltage (E_C) used was the one from carbon (0.277 keV) as the PFSA material backbone is only made of fluorine and carbon. The acceleration voltage (E_0) used for the EDS was 5 kV. Using Castaing's formula we estimated that the spatial resolution depth for the fluorine is 0.670 μm, while for platinum it is 0.79 μm.

3.3. Surface morphology and resistivity

The surfaces of the IPMCs that were produced using the standard and altered recipe were characterized using SEM and atomic force microscopy (AFM) to study the surface roughness and connection between platinum layers. The AFM setup was a ND-MDT aura, operated in semi-contact mode with a cantilever having a radius smaller than 10 nm (Nanosensors), at a frequency of 0.80 Hz and acquiring 256 lines on areas of 1 μm^2 and 10 μm^2 respectively. Sheet resistance of the two samples (diluted and non-diluted) has been measured using the van der Pauw method with a 4-probe station (Cascade 31, Summit) using 400 mV range. The needles of the probe station

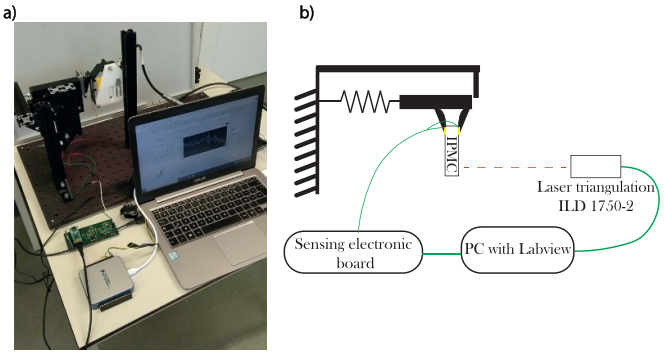

Figure 3. (a) Impulse excitation setup used to characterize the electro-mechanical properties of an IPMC cantilever beam. (b) Schematic of the setup.

were kept at a distance of 1 mm from each other and automatic displacement of the probe station was used with a 1 mm increment in the x and y direction to map the resistivity.

3.4. Sensing electronics and sensitivity

Sensing on IPMCs can be implemented using active or passive methods. Active sensing relies on the fact that the IPMC develops charge imbalance when deformed, measurable via charge, current or voltage measurement circuits [6]. Passive sensing considers the IPMC as a capacitance or resistance, so that when a signal is sent, the drop in resistance or capacitance due to displacement is used as a recording signal. In the first case the IPMC is called active as the material delivers energy while in the second mode the material is considered as a passive element that disturbs the sent signal [6]. Here we have developed an electronic board for sensing the charge produced on the IPMC electrodes [6]. IPMC electrodes are connected through gold contacts to the board input. The first stage of the board is made of a charge amplifier circuit with gain $G = 100$. The signal is sent to an instrument amplifier ($G = 1$), then a second-order passive low-pass filter with cut-off frequency of 1125 Hz is used to filter out high-frequency noise. Data are saved in real-time on a memory card.

Impulse excitation technique (IET) was used to induce controlled displacement to the IPMC cantilever. Oscillations were induced by unit step excitation at the IPMC base, and displacements at the IPMC tip were measured. The unit step excitation was induced through a loaded spring (Thorlabs). Oscillations were measured using a laser displacement sensor (ILD 1750-2 Micro epsilon) and through the developed electronics to extract sensitivity (figure 3). The distance between the laser and the IPMC cantilever was set to 22 cm to keep the beam in the range of detection of the laser. Measurements have been performed on five samples to study repeatability. Prior to the impulse, the IPMC was refilled with PBS solution using a pipette and the measurements have been performed shortly after to maintain the IPMC hydrated and mimic the bio-MEMS environment. The recorded data were further processed with custom Python 3.6 code to extract the oscillation amplitude and natural frequency of the cantilever.

3.5. Young' s modulus estimation and flexural rigidity

Extracting the mechanical parameters of an IPMC is of crucial importance when developing a sensor as mechanical stiffness will influence flexural rigidity. Excitation techniques already have been used to characterize the mechanical properties of IPMC [32]. Upon impulse excitation, the IPMC beam exhibits a damped simple harmonic oscillator behaviour. IETs have been preferred over other characterization techniques since they are recognized as most convenient and non-destructive method to extract mechanical parameters of soft, thin and fragile material [32]. The logarithmic decrement δ (equation (1), y_i being the amplitude of the ith oscillation) can be used to estimate the damping of the system ζ (equation (2)). From the estimation of the damping, the natural frequency w_0 can be estimated using the resonance frequency w (equation (3)).

$$\delta = \frac{1}{n} \ln \frac{y_i}{y_{i+n}} \tag{1}$$

$$\zeta = \sqrt{\frac{\delta^2}{4\pi^2 + \delta^2}} \tag{2}$$

$$w = \sqrt{w_0^2 - 2\zeta^2} \tag{3}$$

$$E = \frac{mL^3}{I} \left(\frac{w_i}{\alpha_i^2} \right)^2 . \tag{4}$$

As reported by Barboni *et al* the Young's modulus E can be estimated using equation (4), with I being the moment of inertia of plain area $I = \frac{BH^3}{12}$, B being the width, H the height, L the length, m the mass and α_i a dimensionless coefficient for the ith resonance frequency of the cantilever beam. The mass of the IPMC has been estimated using a precision balance (Allscales Europe) and the mean value calculated from 15 measurements. About 30 oscillations recorded through the laser triangulation system aforementioned have been used to estimate the resonance frequency of the cantilever. The mean value has been extracted to calculate the Young' s modulus. The flexural rigidity D of the beam have been calculated using the relation $D = EI$.

4. Results and discussion

4.1. Pt distribution

Results for Pt distribution were obtained according to the procedure described in section 3.2. The results for the repeated immersion-reductions steps of the 50 μm-thick Nafion are presented in figure 4. Pt distributions after the first reduction step of 50 μm and 180 μm-thick samples are compared in figure 5. The Pt distribution for Nafion 212 (50 μm thick) using the diluted recipe is shown in figure 7.

4.1.1. Platinum distribution in Nafion 212. Thanks to the high precision of tools and image processing, the effect of repeated immersion-reduction steps can clearly be seen on the pictures of the cross-section for the thin IPMC which went under the

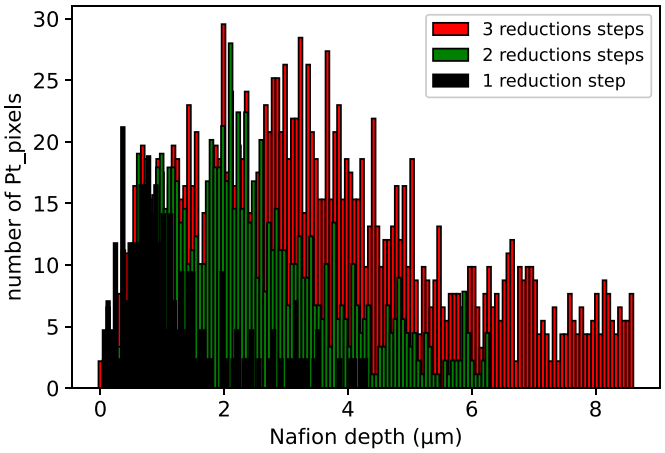

Figure 4. Platinum distribution within the thin Nafion 212 membrane for one (black), two (green) and three (red) reduction steps.

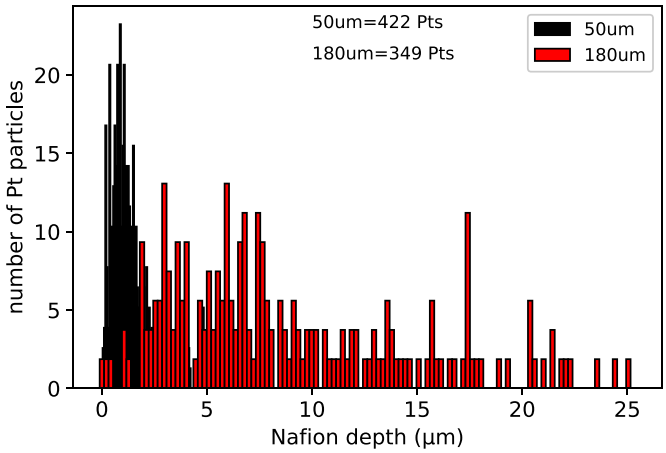

Figure 5. Platinum distribution within thin and thick Nafion after one reduction step (30 mins immersion bath) using standard recipe. Total counts for platinum particles detected for each Nafion membrane.

standard electroless recipe (figure 4). The effect of repeated cycles could hardly be seen on the previously published Pt distribution profiles within standard Nafion [33, 34]. It is apparent from the distributions that the reduction steps follow one another in depth, i.e. the last reduction acts deepest in the membrane while the first reduction happens in proximity of the surface. The overall electrode thickness is about 8 μm (figure 4).

4.1.2. Comparative study of platinum distribution in Nafion 212 and Nafion 117. Interestingly, we could show that the Pt distribution differs strongly in between thin and thick Nafion after one reduction step, while the two samples where immersed in the same immersion bath and reduced in the same reduction bath during the first stage of the initial composition process (figure 5). The number of platinum particles detected is different, meaning that, despite the fact that both samples are coming from the same baths, more platinum was reduced at the interface in the thin Nafion than in the thick Nafion. The difference in Pt distribution is therefore to be correlated with the difference of geometry used (thick versus thin membrane) as both samples are made of the same material with the same equivalent weight. It has been reported in literature that Nafion behaves dynamically in correlation to the electrolyte concentration [35] and that thinner Nafion experiences higher water uptake [36]. Kusoglu *et al* reported that a higher water uptake leads to higher diffusion coefficients in Nafion. Therefore Nafion 212, which has a higher water uptake than Nafion 117, gives rise to a faster reduction close to the surface of the Nafion. In addition, we can hypothesize that PFSA membrane with higher water uptake experiences higher solvation, helping the charged species to move inside the polymer backbone, further promoting interaction between the reducing agent and the reactant to be reduced.

4.1.3. Interpretation of platinum distribution within Nafion 212. As shown by Hsu *et al* in their cluster network model, the ionic channels and networks are bigger and more connected in Nafion that absorbs more water than in the one with smaller water uptake capability [37]. Therefore we hypothesize that the ionic cluster network reorganises differently in the thin Nafion in comparison to the thick Nafion, allowing the chemicals involved in the reduction process to react more on the surface of Nafion (figure 6). Accordingly, thin Nafion has bigger ionic channels and higher connectivity, therefore there are more interactions between the NaBH4 and the Pt organometallic as there is more space for the chemicals to react (figure 6). We hypothesize that bigger and more connected ionic clusters increase the ion mobility, allowing the Pt organometallic from bulk Nafion to migrate toward the surface electrode as well as NaBH4 to react faster with the incoming organometallic. This may explain why platinum is reduced deeper into thick Nafion than in thin Nafion that went through the same immersion bath and reduction step (figure 5). These claims are also in line with the results of Sode *et al*, who studied the influence of parameters on Nafion 117 [20]. They showed that the kinetics of the electroless reaction is mostly dependent on the hydration state of the Nafion. Moreover Millet *et al* reported that the diffusion rate inside the Nafion membrane can be determined by bulk diffusion (M mechanism) or by interfacial diffusion (F mechanism) [33]. Our results suggest that inside Nafion 212 the rate of precipitation is based on the M mechanism as the water uptake capability of the PFSA membrane will mostly influence the diffusion inside the membrane [33].

4.1.4. Platinum distribution in Nafion 212 diluted recipe. Diminishing the concentration of the chemicals allows to reduce the platinum closer to the surface, giving more localized electrodes [39], and alleviating the influence of the diffusion inside the membrane. In the platinum distribution of the final sample that went through the three reductions steps by using the diluted recipe, 75% of platinum is homogeneously localized within 2.62 μm of the Nafion depth (figure 7), while 90% of the particles have been detected within 4.42 μm. It should be pointed out also that the maximum amount of

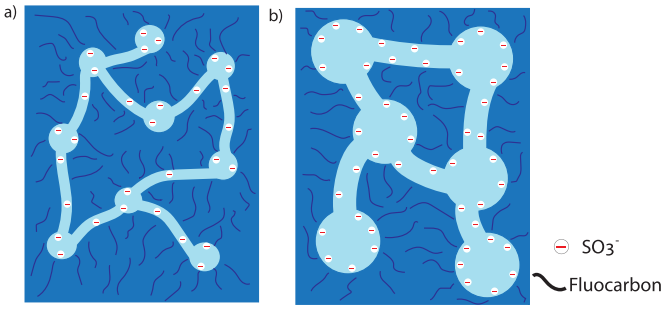

Figure 6. Ionic cluster model in Nafion, (a) Ionic cluster reorganization at low water uptake (b) Ionic cluster reorganization at high water uptake. (Adapted with permission from [38]).

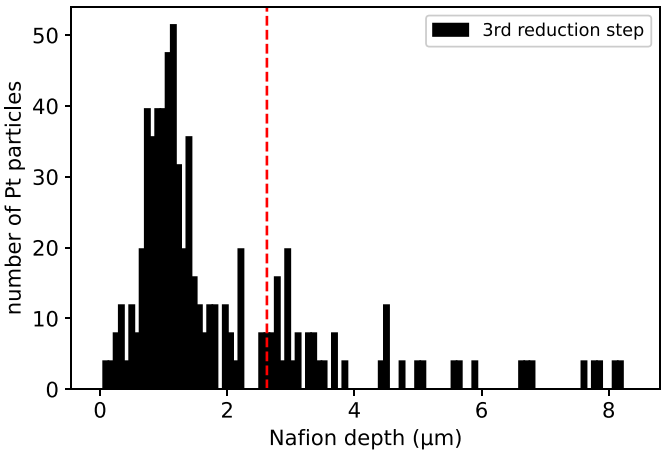

Figure 7. Platinum distribution for the Nafion 212 membrane using the diluted recipe after 3 reductions steps. About 75% of the particles have been detected within 2.62 μm from the surface (red dashed line).

platinum is double the amount detected at the highest peaks for non-diluted recipe (50 instead of 25). Unlike the Nafion 212 that went through the three reduction steps in the non-diluted recipe (figure 4), in the diluted recipe sample the effect of repeated reductions cannot been seen (figure 7). This supports that the platinum deposited during the second and third steps predominantly stays at the interface of the Nafion, most probably on the already grown platinum sites after the first reduction. These results comply with the aforementioned assumptions that the mechanism of precipitation in the Nafion 212 is determined by diffusion inside the membrane (M mechanism) and not by diffusion inside the boundary layer (F mechanism). In addition, by using dilution, we limit the bubbling during the reactions. This helps keeping the thin IPMC sunk into the solution, reducing the fabrication errors inherent to electroless deposition and therefore increasing reproducibility.

4.2. Electrodes

Results for electrodes resistivity and morphology were measured according to section 3.3. The results of the surface morphology of the 50 μm samples that went through the entire manufacturing process using the diluted recipe and non-diluted recipe are shown in figure 8. The sheet resistance

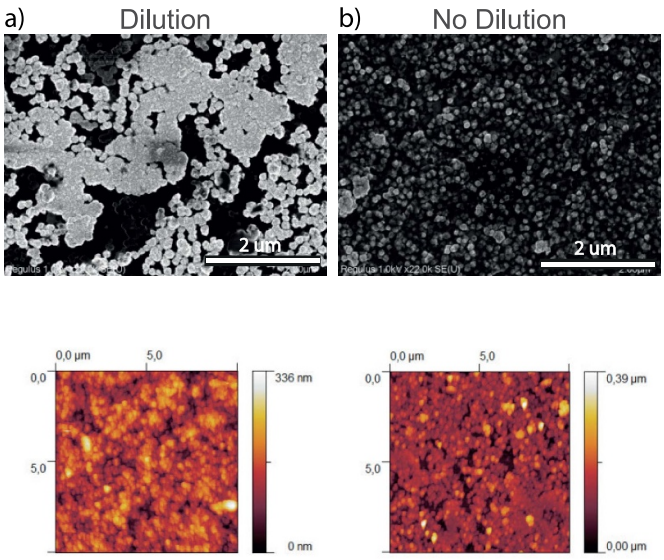

Figure 8. SEM (top) and AFM (bottom) pictures of the surface of 50 μm-thick IPMC after processing with the diluted recipe (a) and the standard recipe (b).

measurements are plotted in a heat map format in figure 9. The conductivity of the electrodes strongly depends on the electroless deposition recipe, as already shown by Shahinpoor and Kim [40]. The final resistivity of the electrodes mostly depends on the initial composition process that grows the first sites of platinum prior to the surface electrodes process. Diminishing the surface resistivity by controlling closely the manufacturing process will lead to a better distribution of the charges along the length of the material and will result in better transducer capabilities [40].

4.2.1. Electrodes morphology. The platinum particles deposited on the surface of the thin Nafion for the diluted recipe showed a homogeneous layer with particles connected together (figure 8(a)). We hypothesize that in this case the growth of the Pt particles is happening within the same plane of the Nafion sheet, due to the dilution.

On the contrary, the thin Nafion with non-diluted recipe showed a non-homogeneous layer with little connection between the Pt particles and grainy look (figure 8(b)). We hypothesize that the reaction predominantly happening at the interface between the Nafion and the reduction bath (F mechanism) leads to the development of the Pt particles in a plane perpendicular to the one of the Nafion sheet. Thus the Pt particles grow in height for the non-diluted recipe while growing in width for the diluted recipe, giving the different appearances (figure 8). It should be pointed out that the root mean square surface roughness for the diluted recipe (51.6 $\pm$ 4.3 nm) is higher than for the non-diluted recipe (39.1 $\pm$ 6.9 nm). The difference might come from the fact that connection of the platinum particles is not complete, leaving large gaps between the Pt particles as seen on the SEM pictures of the diluted recipe (figure 8(a)). On the other hand, the non-diluted recipe leads to a more grainy structure with smaller gaps between

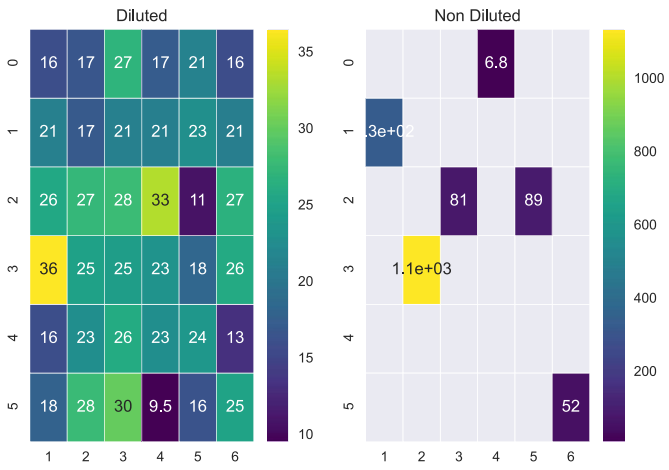

Figure 9. Surface resistance of IPMC samples manufactured using the diluted (left) and non-diluted recipe (right) (values are in $\Omega\,\mathrm{mm}^{-2}$). The blank rectangles indicate open circuits. The x and y axis of the map are the coordinates of the locations of the 4-point measurements with a 1 mm increment in between each point.

the Pt particles, therefore resulting in a lower roughness. Segmentation algorithms have been tested using fixed threshold on the SEM pictures (figures S11 and S12) to extract the number of platinum particle clusters. We have extracted the average number of clusters from the segmented pictures. The results obtained from six pictures shows that the average number of segmented areas is higher for the non diluted than for the diluted (figure S13). The statistics is 168 $\pm$ 101 and 1237 $\pm$ 221 clusters found for the diluted and non diluted recipe respectively, suggesting that the altered recipe leads to the creation of more homogenous platinum electrodes with a higher number of platinum particles being connected, which could explain the lower resistivity.

4.2.2. Sheet resistance. As one can expect from the SEM and AFM images, resistivity is higher for the non-diluted recipe than for the diluted recipe (figure 9). We also noticed during the van der Pauw measurements that many points for the non diluted recipe could not be measured as the resistance was too high (open circuit). The mean value calculated for the sheet resistance of the diluted recipe is $22.06\,\Omega\,\mathrm{mm}^{-2}$ ($N = 36$) with a standard deviation of $5.94\,\Omega\,\mathrm{mm}^{-2}$.

We hypothesize that using the dilution factor on the thin IPMC we obtained better defined sites with platinum being deposited on the surface of Nafion during the initial composition process. Those sites are the ones where the platinum grows during the surface electrodes process, leading to higher connection of the platinum particles. Conversely, for the standard recipe, after the initial composition, the Pt sites are more numerous and more concentrated in the bulk (figure 4).

4.3. Sensing characterization

The oscillations recorded by the laser position system corresponded to the oscillations recorded by the electronics (figures 10(a) and (b), respectively) for the sample number one. Example of responses of samples 2, 3, 4, and 5 have been plotted in supplementary information figures S3–S7 respectively. For each oscillation, the tip displacement (peak-to-peak) measured by the laser triangulation has been correlated to the recorded voltage (peak-to-peak). Mean and standard deviation values were used to compose the responsivity curve (figure 10(c)). Data for 30 oscillations (figure S8) show a good fit with a first-order polynomial ($47.6\,x - 11.6$) ($R^2 = 0.99$). We noticed that dispersion in responsivity was mostly coming from high amplitude oscillations (figure 10(c)). We also noticed that the drying of the thin IPMC increase the dispersion after a few minutes. During the experiments, the water leaves the IPMC, changing the material characteristics (ions mobility) and responsivity. This effect could be avoided when using this material in a wet environment, as it is typically the case for bio-MEMS. The smallest tip displacement detected electrically (960 μm peak- to-peak for a 16 mm-long IPMC) was recorded as a 0.39 mV voltage output (prior to amplification) (red and blue dots in figures 10(a) and (b)). As a comparison, Wang *et al* were able to obtain a 0.32 mV amplitude signal by using a 50 μm-thick IPMC (20 mm long). However Wang *et al* manufactured the thin IPMC in a different way, using electroplating after electroless deposition and Pd based electrodes, known for their lower stiffness [17]. We estimated the response time of the sensor to be in the ms range (figure S2), unfortunately the resolution of the laser as well as the electronics make this value hard to be precisely measured. The calculated sensitivity is $\mathrm{S} = 47.6 \pm 2.0\,\mathrm{mV\,mm}^{-1}$ after amplification ($G = 100$) and $0.476\,\mathrm{mV\,mm}^{-1}$ without amplification, which can be compared to the value found by Khmelnitskiy *et al* ($0.072\,\mathrm{mV\,mm}^{-1}$ without amplification). The authors used a standard IPMC with Nafion 117 [41], showing lower flexibility than our IPMC because of its inherent thickness, which can explain the difference of sensitivity. We also investigated the repeatability by performing the measurements with the same sample after 6 months of storage in water. The response can be seen in supplementary figure S1, interestingly only the first oscillation can be detected. We hypothesized that the handling of the IPMC during the measurement leads to the creation of cracks on the electrode that could explain the lower sensitivity. Creation of cracks already has been reported in the literature as a major hurdle for IPMC [40]. We hypothesized that potential cracks that could happen while using thin IPMC have limited negative effects on dense and homogenous electrodes where the connection between platinum particles is high (figures 8 and 7). By keeping the material in a wet environment in between experiments, we maintain the stress of Nafion low, limiting the deformation and improving the aging of the material. In addition, we can hypothesized that the electrodes with more localized and homogeneous platinum distribution could stay conductive despite high deformation and long-term cycling.

The limit of detection (LOD) is a key figure of merit to assess the performance of the fabricated sensor. The LOD refers to the minimum signal that can reliably be considered as a displacement from the reference position [42, 43]. The LOD with a 90% confidence level is $\mathrm{LOD} = \frac{3\sigma}{S}$, S being the sensitivity of the sensor and σ the standard deviation of noise,

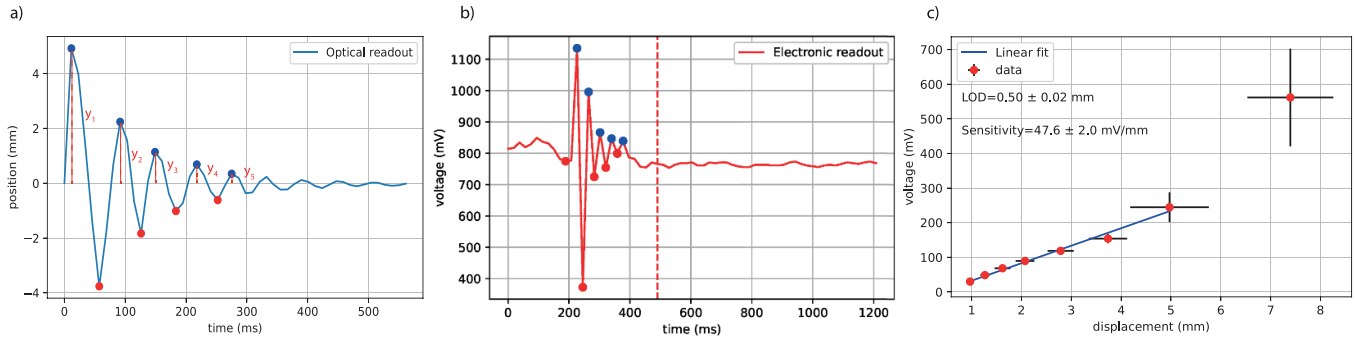

Figure 10. (a) Oscillations of a 50 μm-thick IPMC from diluted recipe recorded through the laser position system. y_i are the points used to compute the logarithmic decrement and damping. The points used to calculate the amplitude are in red and blue. (b) Oscillations of the same IPMC sample recorded through the electronic board ($G = 100$). Points used to calculate the amplitude are in red and blue. Points used to calculate σ (standard deviation of the noise floor) are extracted starting from the red dashed line. (c) Responsivity plot for 50 μm-thick IPMC from diluted recipe for 30 oscillations. Linear fit used to calculate the sensitivity ($R^2 = 0.99$). The response of the sensor without gain can be found in supplementary figure S14.

recorded by the electronics board when the beam its undeflected rest position (figure 10(b) red dashed line). We calculated σ as 7.9 mV, the slope being 47.6 ± 2.0 mV mm^{-1}. Therefore the LOD for our sensor is 500 ± 20 μm.

4.4. Young's modulus estimation and flexural rigidity

The oscillations recorded through the laser were used to estimate the Young's modulus (figure 10(a)). The estimated logarithmic decrement was 0.7082, the estimated damping was 0.1120 ($N = 10$, standard deviation $= 0.06$). The mean of 30 oscillations period was found to be 75 ms, giving a resonance frequency of the beam of 13.2 Hz. In the end, the estimated Young modulus was 550 MPa, a value close to that already found for standard IPMC [6]. We believed that the electroless deposition recipe and final distribution of platinum on the Nafion strongly influence the final Young's modulus of the material as more platinum deposited will lead to a final stiffer IPMC. For our material the Young's modulus is similar that of standard IPMC as the ratio of the thickness of the platinum electrodes deposited over thickness of Nafion is similar for both standard IPMC and thin IPMC manufactured with our recipe.

The flexural rigidity D of our IPMC beam has been calculated to be 3.43×10^{-8} N·m^2. Since the material is 3.6 thinner than standard IPMC, the overall flexural rigidity is largely lower in comparison to standard IPMC as the moment of inertia evolves with the cubic of the beam's height (see section 3.5).

5. Conclusion

We have successfully manufactured a thin IPMC (50 μm thick) for sensing applications using platinum electroless deposition. The difference in platinum distribution for thick and thin IPMC has been shown by comparing the distribution of platinum in Nafion 212 and Nafion 117 that went under the same electroless deposition recipe. We hypothesized that the difference of water uptake explains the difference in Pt distribution for the two samples. Accordingly, the thin polymer is more solvated than the thick one, allowing enhanced displacement of reactants within the polymer backbone and improved ionic cluster reorganization. Overall, reactants have more freedom to distribute and move within the thin Nafion than the thick Nafion. These assumptions suggest that the dynamics of precipitation within thin Nafion is rate determined by membrane diffusion (M mechanism). We have showed that using dilution we can restrain the reaction in order to better control the deposition of Pt on a thin Nafion membrane. The resulting electrodes showed higher conductivity, and higher amount of platinum close to the surface of the PFSA membrane.

Limiting the precipitation reaction by using a dilution factor is the key to manufacture a functional thin IPMC sensor. Constrained electrolyte concentration leads to denser sites during primary plating, which leads to more localized sites for the Pt to be deposited during the following reduction step and final plating. We have characterized the resulting material and showed that it could be used for sensing in the microscale range by means of an active, charge-based sensing setup. In the future, hydrogel materials could be used to create a more compliant layer on top of the thin IPMC sensor for bio-MEMS applications. Additionally, different cations form could be investigated in the future, as already shown for standard IPMC [44]. This aforementioned study showed that the cations form influences the voltage and current amplitudes, thus bigger cations support better sensing properties than small cations. For clarity of the present article and application targeted (bio-MEMS) the focus has been kept on sodium cations, future work could explore the influence of cations types on thin IPMC sensing properties.

This work could represent a milestone for further development of IPMC in different fields. The flexural rigidity of the thin IPMC we obtained is largely lower than for standard IPMC, expanding potential application for sensing. Further investigations could be performed by using different thicknesses of Nafion and different dilution factors in order to obtain a final IPMC with superior sensing capabilities and

actuation capabilities. Interestingly it has been shown that thicker IPMC would show lower back relaxation, future work could study the back relaxation of such a thin material, which is expected to be higher than for standard IPMC [45, 46]. In addition further characterization using different impulse techniques such as controlled sinusoid impulse could help to study the phase response of the material. Fitting the distribution of platinum with existing models on precipitation process within PFSA may provide additional insight. In addition, in order to optimize sensing, electronics could be further investigated that could amplify and filter the recorded signal in the frequency range of interest, depending on the explored application (e.g. humidity, strain or force sensors).

Data availability statement

The data that support the findings of this study are available upon reasonable request from the authors.

ORCID iDs

Paul Motreuil Ragot https://orcid.org/0000-0003-0939-0706
Andres Hunt https://orcid.org/0000-0001-5350-7719
Leandro Nicolas Sacco https://orcid.org/0000-0002-5384-2020

References

[1] Nemat-Nasser S 2002 Micromechanics of actuation of ionic polymer-metal composites *J. Appl. Phys.* **92** 2899–915
[2] Kim K J and Shahinpoor M 2003 Ionic polymer metal composites: II. Manufacturing techniques *Smart Mater. Struct.* **12** 65–79
[3] Bhandari B, Lee GY Ahn SH 2012 A review on IPMC material as actuators and sensors: fabrications, characteristics and applications *Int. J. Precis. Eng. Manuf.* **13** 141–163
[4] Nemat-Nasser S and Wu Y 2003 Comparative experimental study of ionic polymer–metal composites with different backbone ionomers and in various cation forms *J. Appl. Phys.* **93** 5255–67
[5] Bahramzadeh Y and Shahinpoor M 2011 Dynamic curvature sensing employing ionic-polymer–metal composite sensors *Smart Mater. Struct.* **20** 094011
[6] MohdIsa W, Hunt A and HosseinNia S H 2019 Active sensing methods of ionic polymer metal composite (IPMC): comparative study in frequency domain *2019 2nd IEEE Int. Conf. on Soft Robotics (RoboSoft)* pp 546–51
[7] Bahramzadeh Y and Shahinpoor M 2014 A review of ionic polymeric soft actuators and sensors *Soft Robot.* **1** 38–52
[8] Bonomo C, Fortuna L, Giannone P, Graziani S and Strazzeri S 2006 A model for ionic polymer metal composites as sensors *Smart Mater. Struct.* **15** 749–58
[9] Hao M, Wang Y, Zhu Z, He Q, Zhu D and Luo M 2019 A compact review of IPMC as soft actuator and sensor: current trends, challenges and potential solutions from our recent work *Front. Robot. AI* **6** 129
[10] Hitsumoto S, Ihara T and Morishima K 2008 A miniaturized cell stretching tool using ionic polymer metal composite Actuator *MRS Online Proc. Libr.* **1097** 10970303
[11] Motreuil-Ragot P *et al* 2020 Enabling actuation and sensing in organs-on-chip using electroactive polymers *2020 3rd IEEE Int. Conf. on Soft Robotics (RoboSoft)* pp 530–5
[12] Saberi A, Ashworth S and Shahinpoor M 2016 *Ionic Polymer Metal Composites (IPMCs) Substrates as Real Time Sensing Systems to Study Biological Cells Adhesion, Traction and Migration* (American Society of Mechanical Engineers Digital Collection)
[13] Yanamori H, Kobayashi T and Omiya M 2012 *Ionic Polymer Metal Composite (IPMC) for MEMS Actuator and Sensor* (American Society of Mechanical Engineers Digital Collection) pp 417–24
[14] Tsuchitani S, Kikuchi K, Shimizu I, Taniguchi T and Miki H 2016 IPMC actuators fabricated using MEMS technology *Adv. Sci. Technol.* **97** 57–60
[15] Feng G H and Chen R H 2007 Improved cost-effective fabrication of arbitrarily shaped μIPMC transducers *J. Micromech. Microeng.* **18** 015016
[16] Yang L, Wang H and Zhang X 2021 Recent progress in preparation process of ionic polymer-metal composites *Results Phys.* **29** 104800
[17] Wang J, Wang Y, Zhu Z, Wang J, He Q and Luo M 2019 The effects of dimensions on the deformation sensing performance of ionic polymer-metal composites *Sensors* **19** 2104
[18] Lind J U *et al* 2017 Cardiac microphysiological devices with flexible thin-film sensors for higher-throughput drug screening *Lab Chip* **17** 3692–703
[19] Yip J, Feng L S, Hang C W, Marcus Y C W and Wai K C 2010 Experimentally validated improvement of IPMC performance through alternation of pretreatment and electroless plating processes *Smart Mater. Struct.* **20** 015009
[20] Sode A Ingle N J C, McCormick M, Bizzotto D, Gyenge E, Ye S, Knights S and Wilkinson D P 2011 Controlling the deposition of Pt nanoparticles within the surface region of Nafion *J. Membr. Sci.* **376** 162–9
[21] Nakamura T, Ihara T, Horiuchi T, Mukai T and Asaka K 2009 Measurement and modeling of electro-chemical properties of ion polymer metal composite by complex impedance analysis *SICE J. Control, Meas. Sys. Integr.* **2** 6
[22] Oh C , Kim S, Kim H, Park G, Kim J, Ryu J, Li P, Lee S, No K and Hong S 2019 Effects of membrane thickness on the performance of ionic polymer–metal composite actuators *RSC Adv.* **9** 14621–6
[23] Khmelnitskiy I K *et al* 2017 Improvement of manufacture technology and research of actuators based on ionic polymer-metal composites *J. Phys.: Conf. Ser.* **857** 012018
[24] çilingir H D and Papila M 2010 Equivalent' electromechanical coefficient for IPMC actuator design based on equivalent bimorph beam theory *Exp. Mech.* **50** 1157–68
[25] Kusoglu A and Weber A Z 2017 New insights into perfluorinated sulfonic-acid ionomers *Chem. Rev.* **117** 987–1104
[26] Feng C, Li Y, Qu K, Zhang Z and He P 2019 Mechanical behavior of a hydrated perfluorosulfonic acid membrane at meso and nano scales *RSC Adv.* **9** 9594–603
[27] Ingle N J C, Sode A, Martens I, Gyenge E, Wilkinson D P and Bizzotto D 2014 Synthesis and characterization of diverse pt nanostructures in Nafion *Langmuir* **30** 1871–9
[28] Pak J J *et al* 2004 Fabrication of ionic-polymer-metal-composite (IPMC) micropump using a commercial Nafion *Smart Structures and Materials 2004: Electroactive Polymer Actuators and Devices (EAPAD)* vol 5385 (International Society for Optics and Photonics) pp 272–80
[29] Kumar P, Bharti R P, Kumar V and Kundu P P 2018 Chapter 4 - polymer electrolyte membranes for microbial fuel cells: part A. Nafion-based membranes *Progress and Recent*

Trends in Microbial Fuel Cells ed P P Kundu and K Dutta (Amsterdam: Elsevier) pp 47–72
[30] Hawut W, Hunsom M and Pruksathorn K 2006 Platinum electroless deposition on Nafion membrane for PEM fuel cells *Korean J. Chem. Eng.* **23** 555–9
[31] Hosseinabadi P, Javanbakht M, Naji L and Ghafarian-Zahmatkesh H 2018 Influence of Pt nanoparticle electroless deposition parameters on the electrochemical characteristics of Nafion-based catalyst-coated membranes *Ind. Eng. Chem. Res.* **57** 434–45
[32] Biswal D K, Bandopadhya D and Dwivedy S K 2013 Evaluation of electromechanical, damping and dynamic mechanical properties of silver electrode IPMC actuator *Advanced Nanomaterials and Nanotechnology* (*Springer Proceedings in Physics*), ed P K Giri, D K Goswami and A Perumal (Berlin: Springer) pp 321–31
[33] Millet P, Durand R, Dartyge E, Tourillon G and Fontaine A 1993 Precipitation of metallic platinum into Nafion ionomer membranes: I. experimental results *J. Electrochem. Soc.* **140** 1373
[34] Millet P, Pineri M and Durand R 1989 New solid polymer electrolyte composites for water electrolysis *J. Appl. Electrochem.* **19** 162–6
[35] Mauritz K A and Moore R B 2004 State of understanding of Nafion *Chem. Rev.* **104** 4535–86
[36] Fuel Cells etc 2014 Nafion™ membrane comparison table
[37] Hsu W Y and Gierke T D 1983 Ion transport and clustering in Nafion perfluorinated membranes *J. Membr. Sci.* **13** 307–26
[38] Kim R Yuk S, Lee J-H, Choi C, Kim S, Heo J and Kim H-T 2018 Scaling the water cluster size of Nafion membranes for a high performance Zn/Br redox flow battery *J. Membr. Sci.* **564** 852–8
[39] Millet P, Andolfatto F and Durand R 1995 Preparation of solid polymer electrolyte composites: investigation of the precipitation process *J. Appl. Electrochem.* **25** 233–9
[40] Shahinpoor M and Kim K J 2000 The effect of surface-electrode resistance on the performance of ionic polymer-metal composite (IPMC) artificial muscles *Smart Mater. Struct.* **9** 543–51
[41] Khmelnitskiy I K, Gorodilov V V, Kalyonov V E, Lagosh A V and Broyko A P 2018 Investigation of electromechanical parameters of IPMC-sensors *2018 IEEE Conf. of Russian Young Researchers in Electrical and Electronic Engineering* (*IConRus)* pp 411–14
[42] Burgués J, Jiménez-Soto J M and Marco S 2018 Estimation of the limit of detection in semiconductor gas sensors through linearized calibration models *Anal. Chim. Acta* **1013** 13–25
[43] Tang H *et al* 2019 Ultra-high sensitive NO2 gas sensor based on tunable polarity transport in CVD-WS2/IGZO p-N heterojunction *ACS Appl. Mater. Interfaces* **11** 40850–9
[44] Zhu Z, Horiuchi T, Takagi K, Takeda J, Chang L and Asaka K 2016 Effects of cation on electrical responses of ionic polymer-metal composite sensors at various ambient humidities *J. Appl. Phys.* **120** 084906
[45] Porfiri M, Sharghi H and Zhang P 2018 Modeling back-relaxation in ionic polymer metal composites: The role of steric effects and composite layers *J. Appl. Phys.* **123** 014901
[46] Vunder V, Punning A and Aabloo A 2012 Mechanical interpretation of back-relaxation of ionic electroactive polymer actuators *Smart Mater. Struct.* **21** 115023